

Paramagnetic NMR Studies of Blue and Purple Copper Proteins

URSZULA KOLCZAK,¹ JESÚS SALGADO,^{1*} GREGG SIEGAL,¹ MATTI SARASTE,² GERARD W. CANTERS¹

¹ Leiden Institute of Chemistry, Leiden University, Gorlaeus Laboratories, Einsteinweg 55 2333 CC Leiden, The Netherlands

² European Molecular Biology Laboratory, 69012 Heidelberg, Germany

Received 29 March 1999; revised 20 April 1999; accepted 10 June 1999

ABSTRACT: ¹H- and ¹³C-NMR spectroscopy is applied to investigate the Cu_A and type 1 active sites of copper proteins in solution. The analysis of hyperfine shifted ¹H resonances allows the comparison of the electron spin density delocalization in the Cu_A site of the wild-type soluble domains of various cytochrome *c* oxidases (*Thermus thermophilus*, *Paracoccus denitrificans*, and *Paracoccus versutus*) and genetically engineered constructs (soluble domain of quinol oxidase from *Escherichia coli* and *Thiobacillus versutus* amicyanin). Comparable spin densities are found on the two terminal His ligands for the wild-type constructs as opposed to the engineered proteins where the spin is more unevenly distributed on the two His residues. A reevaluation of the Cys H^β chemical shifts that is in agreement with the data published for both the *P. denitrificans* and the *P. versutus* Cu_A soluble domains confirms the thermal accessibility of the ²B_{3u} electronic excited state and indicates the existence of slightly different spin densities on the two bridging Cys ligands. The ¹³C-NMR spectrum of isotopically enriched oxidized azurin from *Pseudomonas aeruginosa* reveals six fast relaxing signals, which can be partially identified by 1- and 2-dimensional (1-D, 2-D) direct detection techniques combined with 3-D triple resonance experiments. The observed contact shifts suggest the presence of direct spin density transfer and spin polarization mechanisms for the delocalization of the unpaired electron. © 1999 John Wiley & Sons, Inc. *Biospectroscopy* 5: S19–S32, 1999

Keywords: azurin; copper A; paramagnetic NMR

INTRODUCTION

Copper is one of the trace elements that plays an essential role in living organisms. Its physiological function depends on the protein with which it is associated and ranges from electron transfer and oxygen transport to active chemistry, such as incorporation of oxygen into substrates.¹ Copper centers can be divided into five categories accord-

ing to their spectroscopic properties. *Type 1* centers occur in blue copper proteins like plastocyanin and azurin, which function as electron carriers.² They are distinguished in the oxidized state by a relatively small hyperfine coupling constant A_{\parallel} ($\sim 50 \times 10^{-4} \text{ cm}^{-1}$, Ref. 3) and intense blue color (maximum absorbance at $\sim 600 \text{ nm}$ with extinction coefficients of $2\text{--}6 \text{ mM}^{-1} \text{ cm}^{-1}$) arising from the S(Cys)–Cu(II) charge transfer transition. In addition to the S^γ of a cysteine, the copper ion is also coordinated by the N^{δ1} atoms of two histidines and the S^δ of a methionine. A fifth ligand, the carbonyl group of a glycine residue, is also present in some blue copper proteins (Fig. 1). X-ray diffraction^{4–9} and NMR studies^{10–13} on sev-

Correspondence to: G. W. Canters (canters@chem.leidenuniv.nl).

* Present address: Institut für Molekularbiologie, Winzerlaer Str. 10, D-07745 Jena, Germany.

Biospectroscopy, Vol. 5, S19–S32 (1999)

© 1999 John Wiley & Sons, Inc.

CCC 1075-4261/99/0S0S19-14

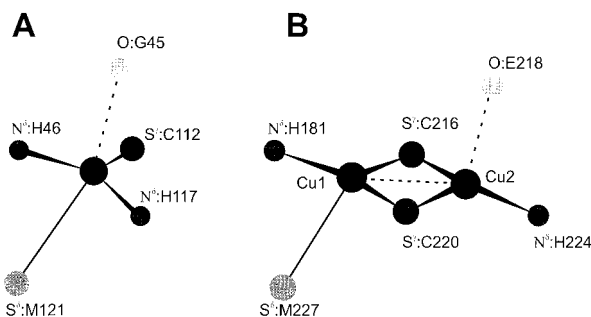


Figure 1. Schematic comparison of the metal site structures of (A) the type 1 copper in *P. aeruginosa* azurin and (B) the Cu_A in the *Paracoccus denitrificans* cytochrome *c* oxidase.

eral type 1 copper proteins showed that they are structurally homologous. The Greek key β -barrel structure typical of these proteins is referred to as the cupredoxin fold. *Type 2* copper sites spectroscopically resemble the aqueous copper(II) ion and have square planar coordination geometries.³ Proteins containing a type 2 copper site are usually involved in substrate binding, for example, superoxide dismutase, which is a superoxide scavenger.¹⁴ Hemocyanin, tyrosinase, and the recently characterized catechol oxidase¹⁵ all contain a pair of antiferromagnetically coupled copper ions, which form a *type 3* copper site that can bind dioxygen. This site is characterized by an absorption band at 330 nm and is EPR silent in the fully oxidized form. Ascorbate oxidase, which catalyzes the reduction of O_2 to H_2O , contains a fourth type of copper center. Spectroscopic characterization showed that ascorbate oxidase contains type 1, 2, and 3 copper sites. However, the crystal structure of ascorbate oxidase revealed that the type 2 and type 3 copper sites are spatially so close that they can be considered as a new *trinuclear copper site*.¹⁶

Cytochrome oxidases contain a so-called Cu_A site in addition to a type 2 copper site.^{17,18} Structural studies of the Cu_A site in the intact cytochrome *c* oxidase proved challenging because of interference from the heme groups and the difficulties of working with a membrane-bound enzyme. A major step forward was achieved via recombinant DNA methods whereby a Cu_A site was introduced into the soluble domain of subunit II of the quinol oxidase from *Escherichia coli* (Cu_A -CyoA).^{19,20} Subsequently, the isolation and expression of Cu_A containing water soluble domains of the cytochrome *c* oxidases from *Bacillus subtilis*,²¹ *Thermus thermophilus* (Cu_A -*Ther*),²² *Paracoccus denitrificans* (Cu_A -*Pde*),²³ and *Para-*

coccus versutus (Cu_A -*Pver*)²⁴ allowed the characterization of a more natively like site.

The similarity between the type 1 copper sites and the Cu_A site was recognized when the primary sequence of subunit II of cytochrome *c* oxidase was determined and compared with the cupredoxins.²⁵ A similar protein fold was suspected, and significant sequence similarities inspired speculations about the close relationship between both types of copper proteins. This similarity was experimentally confirmed by the introduction of a Cu_A center into type 1 copper protein scaffolds (amicyanin and azurin) through the replacement of the short loop that differentiates both copper sites.^{26,27} These engineered proteins have very similar EPR spectra and a purple color as do the isolated Cu_A domains of cytochrome *c* oxidases. The Cu_A site can be considered as a binuclear version of the type 1 copper centers. Schematic drawings of both active centers are depicted in Figure 1. Both copper sites present the same type of strong equatorial ligands (S^γ -Cys and $\text{N}^{\delta 1}$ -His) and weak axial ligands (S^δ -Met and a peptide carbonyl-oxygen in the azurins). Moreover, these ligands are arranged around the copper in a similar coordination geometry as if a set of common characteristics had been selected for performing an efficient electron transfer function. Distorted tetrahedral geometry, strong binding to thiolate sulfur ligands (which imposes a high degree of electron delocalization), and weak axial bonding interactions have all been discussed extensively in the literature as the main determinants of the electronic structure and the electron transfer characteristics of these copper proteins.^{28–31} Although these properties are common to the type 1 and the Cu_A sites, they are highlighted in the second because of their higher nuclearity.^{31,32} The Cu_A site, which acts as a one electron redox center, is mixed valence in its oxidized state ($\text{Cu}^{1.5}\text{–Cu}^{1.5}$) with the result that the copper ions are magnetically indistinguishable.^{33–35}

In the blue and purple copper centers the profound interaction between the copper ions and their ligands in the oxidized state is reflected in the amount of spin density delocalized over these ligands. Consequently, EPR and paramagnetic NMR techniques appear to be the methods of choice for studying the electronic and magnetic properties of active sites in these proteins. However, NMR studies of oxidized copper complexes encounter considerable problems that are due to the slow electronic relaxation of the $\text{Cu}(\text{II})$ ion that induces a large line broadening on the signals of nuclei in the metal ligating residues or

those in close proximity to the metal center.³⁶ These difficulties have been partially overcome for *blue copper* proteins that have favorable rates of electron self-exchange by using the water-eliminated Fourier transform (WEFT) filter³⁷ and exchange spectroscopy or saturation transfer experiments on samples containing both oxidized and reduced forms of the protein.^{38–40} The electronic relaxation of the Cu_A containing proteins is much more favorable for NMR studies (about 100 times faster) than in mononuclear copper complexes,⁴¹ thus allowing detection of the hyperfine shifted resonances in ¹H spectra. Indeed, NMR has been used to study the spectroscopic properties of Cu_A sites in a number of Cu_A containing proteins.^{24,42–45} However, a number of unresolved issues remained. The paramagnetically shifted signals originating from the H^β protons of the cysteine ligands require more detailed study, because of the importance of the information derived from their analysis. Moreover, conspicuous variations in the shift patterns of the signals for the histidine ligands have been observed that until now have found no satisfactory explanation. Here we report new data on the Cu_A site in the quinol oxidase construct of *E. coli*.^{19,20} With these data at hand, along with data reported in the literature on different wild-type and engineered Cu_A sites, a fruitful comparison can be made. This allows a deeper understanding of the electronic structure properties of the Cu_A site and the definition of different patterns of electron delocalization corresponding to different Cu_A sites.

A possibility to considerably extend the amount of NMR information available from Cu(II) active sites is offered by the development of ¹⁵N and ¹³C enrichment protocols. Given an equal metal–nucleus distance and the same spatial coordinates, the contact and pseudocontact shifts are both independent of the type of resonating nucleus.⁴⁶ However, the paramagnetic contribution to relaxation is scaled by a factor of $(\gamma_I/\gamma_H)^2$, which favors ¹⁵N and ¹³C detection over ¹H detection for the residues in the immediate vicinity of the paramagnetic center. For nuclei further than approximately 9 Å from the copper ion, assignment strategies based on the through bond connectivities between ¹⁵N, ¹³C, and ¹H nuclei observed in triple resonance experiments can be applied in a manner similar to diamagnetic proteins.

The second set of questions that we address in the present work are whether we can obtain valuable information from solution NMR studies on paramagnetic copper centers, even when the elec-

tron relaxation rates are unfavorable, and how close to the natural copper active sites that we can investigate without recourse to metal substitution. Some of the answers to these questions are illustrated by ¹³C-NMR studies of isotopically enriched azurin, which we used as a test case for this type of experiment.

PARAMAGNETIC SHIFTS

For paramagnetic compounds the total observed chemical shift can be factored into contributions from diamagnetic, contact, and dipolar terms as shown below^{47–49}:

$$\delta^{\text{tot}} = \delta^{\text{dia}} + \delta^{\text{con}} + \delta^{\text{dip}} \quad (1)$$

The contact contribution, δ^{con} , results from the direct delocalization of the unpaired spin onto the ligands and is given by

$$\delta_j^{\text{con}} = \frac{A^j/h}{3\beta\gamma/2\pi} \left(\frac{\chi_{xx}}{g_{xx}} + \frac{\chi_{yy}}{g_{yy}} + \frac{\chi_{zz}}{g_{zz}} \right) \quad (2)$$

where χ_{ii} and g_{ii} ($ii = xx, yy, zz$) are the principal components of the paramagnetic susceptibility tensor χ and the spectroscopic splitting \mathbf{g} tensor, respectively; β is the Bohr magneton; γ is the gyromagnetic ratio of the nucleus j ; and A^j/h measures the Fermi contact interaction between the nucleus j and the unpaired electron spin.

The third contribution to δ^{tot} comes from the dipolar or through-space interaction δ^{dip} , which arises from the anisotropy in the paramagnetic susceptibility tensor and influences signals from both ligated and nonligated residues according to the relationship

$$\delta_j^{\text{dip}} = \frac{1}{12\pi r^3} [\Delta\chi_{\text{ax}}(3 \cos^2 \theta - 1) + 1.5\Delta\chi_{\text{rh}}(\sin^2 \theta \cos 2\phi)] \quad (3)$$

where θ and ϕ are the spherical polar coordinates of the nucleus j relative to the principal axes of the χ tensor and r is the distance between the nucleus and the unpaired electron. The axial ($\Delta\chi_{\text{ax}}$) and rhombic ($\Delta\chi_{\text{rh}}$) magnetic susceptibility anisotropy values are given by

$$\Delta\chi_{\text{ax}} = \chi_{zz} - 0.5(\chi_{xx} + \chi_{yy}) \text{ and } \Delta\chi_{\text{rh}} = \chi_{xx} - \chi_{yy}$$

Cu_A ACTIVE SITE BY ¹H-NMR

Nuclear Hyperfine Couplings and Electronic Structure of Cu_A

Knowledge of the detailed features of the geometrical and electronic structure of the Cu_A site is essential to understand the origin of the subtly balanced properties of this site and their connections with its function. Significant efforts were made in the last few years in this direction. Molecular orbital calculations using simplified models of dinuclear mixed valence copper complexes were performed that were guided by structural data and EPR, electron nuclear double resonance (ENDOR), circular dichroism (CD), magnetic CD (MCD), and resonance Raman (RR) spectroscopic data on mixed-valence model complexes and Cu_A proteins.^{30,31,50–53} From these studies the electronic structure of the Cu_A site and mixed-valence model complexes was defined in which the highest occupied molecular orbital (HOMO) is a σ_u^* (b_{3u}) orbital in the case of the Cu_A and a π_u (b_{2u}) orbital in the case of the mixed-valence model complexes.^{30,31} The presence of a different orbital ground state in these two systems is mainly due to the larger compression of the CuS₂Cu diamond core and the closer Cu–Cu distance in the Cu_A proteins.³¹ A complementary view was provided by NMR studies,^{24,42–45} which allowed the study of the electron-spin distribution in a number of different Cu_A proteins and the unambiguous identification of the electronic ground state for the Cu_A site of the soluble domain of the *Paracoccus* cytochrome *c* oxidase as a ${}^2B_{3u}$ state.²⁴ Additionally, based on the analysis of the temperature dependence of ¹H-NMR hyperfine shifts, Salgado et al. proposed that the ${}^2B_{3u}$ excited state is thermally accessible at room temperature.²⁴

Electron-Spin Distribution in Cu_A Site: Equivalency of Histidines

The paramagnetic effect on the NMR of nuclei around the Cu_A site was used to map the electron-spin distribution in the copper ligands. From NMR^{24,42,44,45} and ENDOR⁵² data collected for various Cu_A proteins it can be estimated that large amounts of spin density are delocalized to the Cys bridging ligands (~ 20% each). The spin density in the imidazole His ligands is moderate (~ 4%), while negligible spin density is delocalized to the weak axial ligands. ¹H-NMR spectra were measured and assigned for a Cu_A containing an amicyanin mutant (from *Thiobacillus versu-*

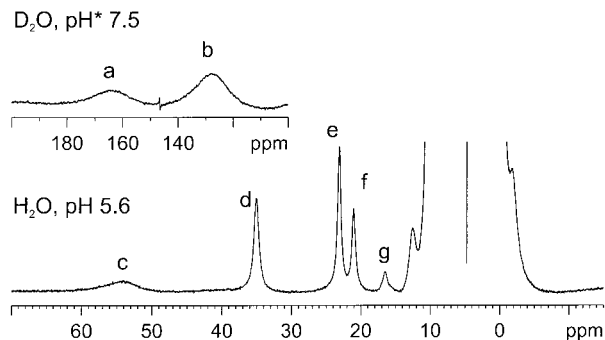


Figure 2. The 1-D ¹H-NMR spectrum of the mixed valence Cu_A-CyoA. Applying the same assignment strategy as for Cu_A-Pver,²⁴ the characteristic peaks of the spectrum are identified as follows: peak d, α -His181C^{δ2}H; peak e, His224C^{δ2}H; peak f, His181N^{ε2}H; peak g, His224N^{ε2}H. (The numbers refer to the sequence of the complete subunit II of the *Paracoccus* cytochrome *c* oxidase.) Peaks a–c belong to the H^β of the coordinated Cys residues. (A sequence-specific assignment of these signals has not been successful to date.)

tus, Cu_A-ami)⁴⁴ and for Cu_A-Ther,⁴² Cu_A-Pde,⁴⁵ and Cu_A-Pver.²⁴ Additionally, we recently measured and partially assigned the ¹H-NMR spectrum of Cu_A-CyoA, which is shown in Figure 2. When the paramagnetic regions of these spectra are carefully compared, we observe that, although the overall patterns are similar, significant differences do emerge. We focus first on resonances from the coordinated histidines for which the measured shifts in different Cu_A proteins are collected in Table I.

Because of the complexity of the spin-density transfer mechanisms in coordinated imidazole rings, which include both σ and π delocalization,^{36,48,49,54} a detailed calculation of the hyperfine couplings and spin densities in the His ligands is difficult and is not attempted at this point. Here we restrict ourselves to rationalizing the most important differences found experimentally. The Cu_A-Ther can be used as the starting reference for our comparison because in this case protons at analogous positions of the two imidazole rings exhibit similar shifts (see Table I). Bertini et al. concluded from this observation that in the Cu_A-Ther both coordinated histidines are equivalent.⁴² In the *Paracoccus* proteins, however, the His 181 C^{ε1}H resonance was not found. The reasons for this are not clear. It can be argued that the missing proton might not be shifted enough and lies hidden inside the diamagnetic protein envelope where it would not be easily detected via the nuclear Overhauser effect (NOE)

Table I Experimental ^1H Chemical Shifts (ppm) from Coordinated His-imidazole Rings of Different Cu_A Proteins

	His 181				His 224			
	$\delta\text{C}^{\delta 2}\text{H}$	$\delta\text{N}^{\epsilon 2}\text{H}$	$\delta\text{C}^{\epsilon 1}\text{H}$	$(\delta^{\delta 2} + \delta^{\epsilon 2})/2$	$\delta\text{C}^{\delta 2}\text{H}$	$\delta\text{N}^{\epsilon 2}\text{H}$	$\delta\text{C}^{\epsilon 1}\text{H}$	$(\delta^{\delta 2} + \delta^{\epsilon 2})/2$
$\text{Cu}_A\text{-Pde}^a$	28.3	24.2	NO	26.2	28.6	27.3	19.1	28.0
$\text{Cu}_A\text{-Pver}^b$	28.5	24.3	NO	26.4	28.7	27.2	19.2	28.0
$\text{Cu}_A\text{-Ther}^c$	34.0	26.0	22.0	30.0	30.0	25.0	17.0	27.5
$\text{Cu}_A\text{-ami}^d$	38.5	28.7	27	33.6	24.0	22.0	15.5	23.0
$\text{Cu}_A\text{-CyoA}^e$	36.0	22.0	NO	29.0	24.0	17.0	NO	20.5

The numbers of the residues refer to the sequence of the complete subunit II of the *Paracoccus* cytochrome *c* oxidase. NO, not observed.

^a 278 K; pH 6.5; data are from Ref. 45.

^b 278 K; pH 5.4; data are from Ref. 24.

^c 278 K; pH 8.0; data are from Ref. 42.

^d 280 K; pH 6.0; data are from Ref. 44.

^e 278 K; pH 5.6; data are from the spectrum in Figure 2.

because of overlap and line-broadening problems. This argument could lead to the conclusion that the spin density in His 181 is smaller than in its partner His 224. However, the rest of the His 181 imidazole–proton shifts of $\text{Cu}_A\text{-Pde}$ and $\text{Cu}_A\text{-Pver}$ are very similar to those of His 224 (Table I). Moreover, it is well known that the His $\text{C}^{\epsilon 1}\text{H}$ protons of histidines coordinated via the $\text{N}^{\delta 1}$ are not good reporters of the total spin density in this ligand, because for these protons positive and negative spin-density transfer effects can effectively compensate each other, leading to small or no net shifts.^{36,46} Thus, we base our discussion of the various Cu_A sites on a comparison of the shifts of the His $\text{C}^{\delta 2}\text{H}$ and $\text{N}^{\epsilon 2}\text{H}$ protons whose values are more consistent. In this way we find that the Cu_A histidine proton signals of the three wild-type Cu_A proteins ($\text{Cu}_A\text{-Pde}$, $\text{Cu}_A\text{-Pver}$, and $\text{Cu}_A\text{-Ther}$) exhibit shifts of similar magnitude. This holds when we compare the two histidines of one protein with each other and when we compare corresponding histidines of the three different proteins. A convenient measure to judge similarities is the average shift of the $\text{C}^{\delta 2}\text{H}$ and $\text{N}^{\epsilon 2}\text{H}$ protons, which amounts to 27.7 ppm for the two histidines of the three wild-type Cu_A proteins (Table I). Thus, this value, which should be proportional to the spin density on the histidine ligands, is characteristic of the ^1H -NMR spectra of the wild-type Cu_A soluble domains. This analysis also indicates that in these systems the two histidines are roughly equivalent.

Continuous wave (CW) ENDOR spectra of the wild-type Cu_A site of nitrous oxide reductase also show a single ^{14}N coupling that could again be due to the equivalence of the two coordinated

histidines.⁵² For the $\text{Cu}_A\text{-ami}$ and $\text{Cu}_A\text{-CyoA}$ proteins, however, a clear reduction of 25% is observed in the shifts of His 224* (The sequence number here and throughout the rest of the text refers to the complete subunit II of the *Paracoccus* cytochrome *c* oxidase. For simplicity, we used the same numbering scheme for the homologous residues in the rest of the Cu_A proteins discussed in this article, which are indicated by an asterisk following the residue number.) The average shift for this residue is now ~ 21.7 ppm, while the average shift for His 181* is increased significantly to 31.3 ppm (Table I). These differences indicate that the two coordinated histidines are not equivalent in the two engineered Cu_A proteins. It appears that the amount of spin density delocalized in the Cu_A His ligands varies among different Cu_A proteins, ranging from the equivalent histidines of the wild-type Cu_A proteins to the inequivalent ones in the engineered proteins. This conclusion must be treated with caution however. ENDOR studies on the natural Cu_A site of the complete mitochondrial cytochrome *c* oxidase from bovine heart, for instance, show different spin densities in the two His ligands.⁵⁵ We should also bear in mind that the wild-type Cu_A proteins discussed here are soluble-domain protein constructs whose structure and electronic properties might not be the same as those of the corresponding complete cytochrome *c* oxidases.

Equivalency of Coppers

What is the origin of the differences in the histidine spin densities pointed out above? Different spin densities in the histidine rings can be due to

different strengths of coordination to the metal ions or different orientations of the histidine rings with respect to the CuS_2Cu core. Another possibility is that the unpaired spin densities on each of the two copper ions are different. (One should keep in mind that each of the two copper ions coordinates only one of the two histidines; see Fig. 1.)

The self-consistent field- $X\alpha$ -scattered wave (SCF- $X\alpha$ -SW) molecular orbital calculations using the bovine heart cytochrome *c* oxidase Cu_A structure show a slightly asymmetrical charge distribution for the two coppers (32 versus 39%) that corresponds to different spin densities in the ligating histidine residues (1.1 versus 1.9%, respectively).³¹ As can be seen from the data presented in Table I, valence delocalization appears to be more extensive in the natural Cu_A soluble domains than in the two engineered Cu_A proteins Cu_A -ami and Cu_A -CyoA. In the latter case partial valence trapping was also proposed from the analysis of EPR, optical absorption, CD, and MCD spectroscopic data and was tentatively correlated with stronger coordination of the back bone carbonyl axial ligand as found in the crystal structure of this protein.^{56,57} Valence trapping was proposed as the explanation of the experimental observation in the high pH form of the Cu_A -*Pver*,²⁴ Cu_A -*Pde*, and the His224Asn mutant of the latter protein. Structural information is needed to improve our understanding of the spin distribution over the Cu_A site.

NMR Properties of Cys Residues

The H^β resonances of the cysteine bridging ligands of the Cu_A -*Pver* were used as reporters of the electronic structure properties of the Cu_A site.²⁴ Two aspects of these resonances were analyzed: the apparently anomalous spread of the hyperfine shifts and the complex temperature-dependent behavior. The large differences in the hyperfine couplings of the four Cys H^β protons arise from their different orientations with regard to the orbital containing the unpaired electron.^{24,52} A qualitative analysis on the basis of a Karplus-type relationship for the ^1H hyperfine coupling in as a function of the dihedral angle reproduces the spread of the Cys H^β hyperfine couplings in agreement with the crystallographic $\text{S}^\gamma\text{-S}^\gamma\text{-C}^\beta\text{-H}^{\beta 1}$ dihedral angles⁵⁸ and a $^2\text{B}_{3u}$ (σ_u^*) ground state.^{24,52} In addition, the marked temperature dependence of the Cys H^β hyperfine shifts (unexpectedly large positive slopes for the $\text{H}^{\beta 2}$ protons and negative slopes for the $\text{H}^{\beta 1}$ pro-

tons of the Cys 216 and Cys 220 in the Curie plots^{24,42,45}) was successfully simulated by taking into account a partial population of the $^2\text{B}_{3u}$ (π_u) excited state according to a Boltzmann distribution. From this analysis it was concluded that the $^2\text{B}_{3u}$ excited state lies 350 cm^{-1} above the $^2\text{B}_{3u}$ ground state²⁴ which is about 1 order of magnitude less than theoretical estimates.^{30,31}

An independent NMR study was also performed on the closely related Cu_A soluble domain from *P. denitrificans*.⁴⁵ In this case the Cys H^β resonances, which are very hard to detect due to their large linewidth, were observed in ^2H -NMR spectra of Cu_A -*Pde* with specifically deuterated cysteines. Three of the Cys H^β signals appear at almost identical positions for both the Cu_A -*Pde*⁴⁵ and Cu_A -*Pver*²⁴ (48.6, 205, and 300 ppm at 278 K). These signals also show identical temperature dependencies. Although the reported sequence-specific assignment of these resonances is different for the two *Paracoccus* proteins, the assignment made for the Cu_A -*Pver* is more reliable, because it was based on unambiguous NOE connectivities.²⁴ A fourth Cys H^β found in the ^2H -NMR spectrum of Cu_A -*Pde* at 445 ppm⁴⁵ was not observed in the ^1H -NMR spectrum of Cu_A -*Pver*. Instead, a very broad signal at ~ 250 ppm was found for this latter protein.²⁴ Although this ~ 250 ppm feature makes the appearance of the NMR spectrum in the 300–200 ppm region more similar to the spectrum of the Cu_A -*Ther*,⁴² the large broadening of this signal does not correlate with its hyperfine shift. Additionally, no NOE relating this signal to any other in the NMR spectrum could be observed. Preliminary pulsed-ENDOR experiments on the Cu_A -*Pver* showed a large ^1H hyperfine coupling of ~ 17 MHz, which is in good agreement with the 445 ppm Cys H^β shift observed in the ^2H -NMR spectrum of Cu_A -*Pde* (J. Salgado, M. van Gastel, E. Groenen, G. W. Canters, unpublished results). Thus, this latter resonance might correspond to the Cys220 $\text{H}^{\beta 2}$.

We considered the possibility that Cys220 $\text{H}^{\beta 2}$ resonates at 445 ppm and reanalyzed the temperature dependence of the Cu_A -*Pver* Cys H^β . We used the temperature-dependence data reported by Luchinat et al. for the 445 ppm signal of the Cu_A -*Pde*.⁴⁵ Figure 3 shows the Cys H^β couplings (A/h in MHz) versus the inverse absolute temperature calculated with Eq. (4)²⁴:

$$\left(\frac{A_{\beta i}}{h}\right) = \frac{(b_1 \sin^2 \phi_{\beta i} + c_1) + e^{-\Delta E/kT}(b_2 \cos^2 \phi_{\beta i} + c_2)}{(1 + e^{-\Delta E/kT})} \quad (4)$$

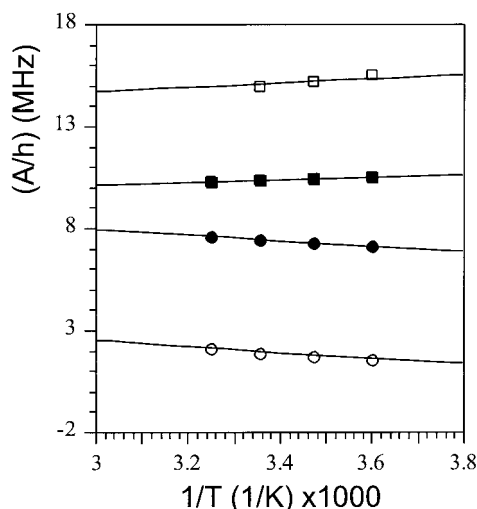


Figure 3. Experimental temperature dependence of the Cys H^β hyperfine shifts and theoretical fitting according to Eq. (4). (○) Cys220 $H^{\beta 1}$, (●) Cys216 $H^{\beta 1}$, (■) Cys216 $H^{\beta 2}$, and (□) Cys220 $H^{\beta 2}$. Data for the Cys220 $H^{\beta 2}$ were taken from the study on the Cu_A -*Pde* by Luchinat et al.⁴⁴ The rest are data from the Cu_A -*Pver*.²⁴

where $\phi_{\beta i}$ ($i = 1, 2$) is the S^γ - S^γ - C^β - $H^{\beta i}$ torsion angle; the subscripts 1 and 2 refer to the orbital ground (σ_u^*) and excited (π_u) states, respectively; and b_j and c_j ($j = 1, 2$) are constants proportional to the spin density on the Cys S^γ . The theoretical curve reproduces the experimental data using the same values of the angles $\phi_{\beta i}$ as in the previous analysis.²⁴ The only significant change is an increase in the value of b_1 (from 14.5 to 22.7 MHz), while the rest of the b_j and c_j constants do not change appreciably (see Table II). The value of $\Delta E = 350 \text{ cm}^{-1}$ is the same as reported previously.²⁴

The value found for b_1 is in agreement with a $\sim 20\%$ spin density on the Cys220 S^γ . There were intriguing differences for the constants b_j and c_j between the ground and excited states and between the two cysteine residues.²⁴ Because b_j constants are proportional to the spin densities on the Cys S^γ , it is worth pointing out that the observed differences in the b_1 values for Cys 216 and Cys 220 may be an indication of a significantly larger amount of spin density on the Cys 220 residue in the ground state, while the b_2 values indicate a slightly larger spin density in the excited state at Cys 216 (see Table II).

BLUE COPPER: ^{13}C -NMR INVESTIGATION

Triple Resonance Spectroscopy: Limitations Due to Paramagnetic Relaxation

Sequence-specific assignments for uniformly doubly labeled [^{13}C , ^{15}N] *P. aeruginosa* azurin were obtained from the following triple resonance NMR experiments: HNCACB,⁵⁹ HNCA,^{60,61} CBCA-(CO)NH,⁶² and HNCO,⁶³ which correlates $^{13}\text{C}^\beta/\text{C}^\alpha(i)$ - $^{15}\text{N}(i)$ -NH(i) and $^{13}\text{C}^\beta/\text{C}^\alpha(i-1)$ - $^{15}\text{N}(i)$ -NH(i), $^{13}\text{C}^\alpha(i)$ - $^{15}\text{N}(i)$ -NH(i) and $^{13}\text{C}^\alpha(i-1)$ - $^{15}\text{N}(i)$ -NH(i), $^{13}\text{C}^\beta/\text{C}^\alpha(i-1)$ - $^{15}\text{N}(i)$ -NH(i), and $^{13}\text{CO}(i-1)$ - $^{15}\text{N}(i)$ -NH(i), respectively. Assignment of the backbone ^{15}N , ^{13}C , and ^1H nuclei was made for 126 out of 128 residues in the reduced, diamagnetic Cu(I) *P. aeruginosa* azurin and for 100 residues in the oxidized-paramagnetic Cu(II) *P. aeruginosa* azurin (U. Kolczak, G. D. Siegal, and G. W. Canters, manuscript in preparation). The residues whose signals were not observed in the 3-D data sets from oxidized azurin belong to

Table II Angles and Constants of Eq. (4) Obtained after Fitting Hyperfine Couplings of Cu_A Cys H^β Protons at Different Temperatures

Nucleus	A/h at 298 K (MHz)	$\phi_{\beta i}^a$ (°)	$\phi_{\beta i}^b$ (°)	b_1 (MHz)	b_2 (MHz)	c_1 (MHz)	c_2 (MHz)	$b = (0.82b_1 + 0.18b_2)^c$ (MHz)	ρ_s^d
C216 $H^{\beta 1}$	7.5 ^e	78 (78)	92	10.3	31.0	0.2	0.5	14.26	0.14
C216 $H^{\beta 2}$	10.5 ^e	-41 (-35)	-28						
C220 $H^{\beta 1}$	2.1 ^e	108 (114)	111	22.7	23.0	-0.4	-0.5	22.75	0.23
C220 $H^{\beta 2}$	15.0 ^f	-11 (-12)	-9						

^a S^γ - S^γ - C^β - $H^{\beta i}$ dihedral angles from the crystal structures of *P. denitrificans* cytochrome *c* oxidase⁵⁸ and Cu_A -CyoA.⁵⁶

^b S^γ - S^γ - C^β - $H^{\beta i}$ dihedral angles from the fitting using Eq. (4).

^c Weighted average of b_1 and b_2 according to a Boltzmann distribution. An 18% population of the excited state is considered for $T = 298 \text{ K}$ and $\Delta E = 350 \text{ cm}^{-1}$.

^d $\rho_s = b/B$, assuming $B = 100 \text{ MHz}$.

^e From the ^1H -NMR spectrum of Cu_A -*Pver*.²⁴

^f From the ^2H -NMR spectrum of Cu_A -*Pde*.⁴⁵ A similar value was obtained from pulsed-ENDOR on the Cu_A -*Pver* (unpublished results).

the following regions: region 1, residues 10–15; region 2, residues 35–36; region 3, residues 44–48; region 4, residues 87–90; and region 5, residues 112–118 and 120–122. The amino acids in close vicinity to the copper ion (regions 1, 3, and 5) are experiencing line broadening due to electron–nuclear dipolar interaction and in the ligating residues additional scalar interaction. Therefore, signals from these 15 residues could not be observed in any of the 3-D spectra that were recorded so far using “diamagnetic conditions.” The absence of signals from the remaining residues in regions 2 and 4 originates mainly from conformational, rather than paramagnetic, effects. Comparison of the X-ray structures of the *P. aeruginosa* azurin determined at low and high pH⁸ revealed local conformational changes related to the protonation and deprotonation of residue His 35. The most affected residues are Pro 36 and Gly 37. When His 35 changes its protonation state the peptide bond between residues 36 and 37 flips, which in turn causes a movement of the loops containing residues 9–12 and 88–91. The ¹⁵N relaxation data obtained using the reduced form of azurin⁶⁴ is in very good agreement with this observation. The exchange between protonated and unprotonated conformation is slow on the NMR time scale.^{65,66} Use of solution conditions close to the p*K*_a value gives rise to two sets of NMR signals whose intensities are proportional to the amount of each form present. The p*K*_a for the reduced form was determined to be 7.3,^{67,68} while for the oxidized protein only an approximate value of 6.0 ± 0.4 was reported.⁶⁹ The 1-D ¹H-NMR spectrum of the oxidized azurin at pH 5.12 exhibits a well-resolved, slowly relaxing signal *X* at 11.04 ppm [Fig. 4(A)], which upon a change of pH to 7.18 shifts to 11.59 ppm *X'* [Fig. 4(B)]. From the triple resonance experiments (pH 5.5) we could correlate the resonance at 11.04 ppm to the amide proton of Asn 38, which not surprisingly, experiences changes in the local magnetic field upon rearrangement of the neighboring peptide bond. We followed the relative intensity of signals *X* and *X'* during a pH titration from 4.0 to 9.0. Using this titration data the p*K*_a of the *X*–*X'* interconversion was determined to be 5.94. A very similar p*K*_a value was reported for the Co(II) and Ni(II) derivatives of *P. aeruginosa* azurin.⁷⁰ In Figure 4(C) the spectrum recorded at pH 5.92 contains the *X* and *X'* resonances with almost equal intensities. The presence of two forms related to the titration of His 35 and the conformation of the 36–37 peptide bond reduces the sensitivity of the triple resonance experi-

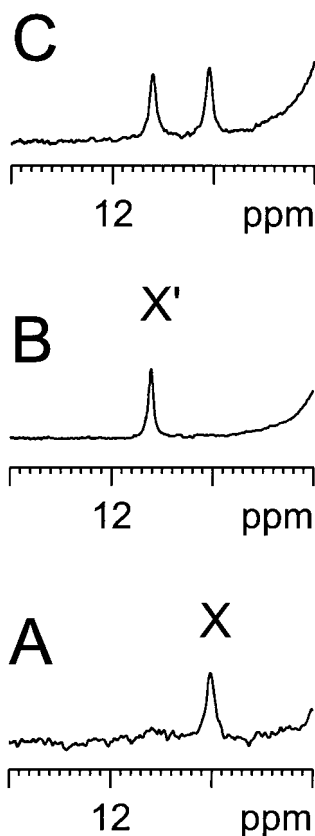


Figure 4. The 1-D ¹H-NMR spectra of *P. aeruginosa* azurin in 25 mM potassium phosphate buffer 95 : 5 H₂O : D₂O at 40°C and pH (A) 5.12, (B) 7.18, and (C) 5.92 that were collected at 0.75 scans/s and apodized with exponential 3-Hz line broadening. Peaks *X* and *X'* correspond to the NH of residue Asn 38 in the His 35 protonated and unprotonated form of the protein.

ments acquired at pH 5.5 by a factor of 4 and explains the loss of the signal for the residues located in regions 1, 2, and 4. Because residues from loops 10–15 are at an intermediate distance from the copper ion, paramagnetic effects will also play a role in the loss of signal. A detailed report on these results, as well a comparison between both oxidation states, will be presented elsewhere (U. Kolczak, G. D. Siegal and G. W. Canters, manuscript in preparation).

Use of ¹³C Direct Detection

Figure 5 compares the 1-D ¹³C-NMR spectra of the reduced (trace A) and oxidized (trace B) forms of the doubly labeled *P. aeruginosa* azurin. Six resolved peaks (labeled A–F) can be detected that appear to be paramagnetically affected. We need to point out that at this stage we cannot exclude

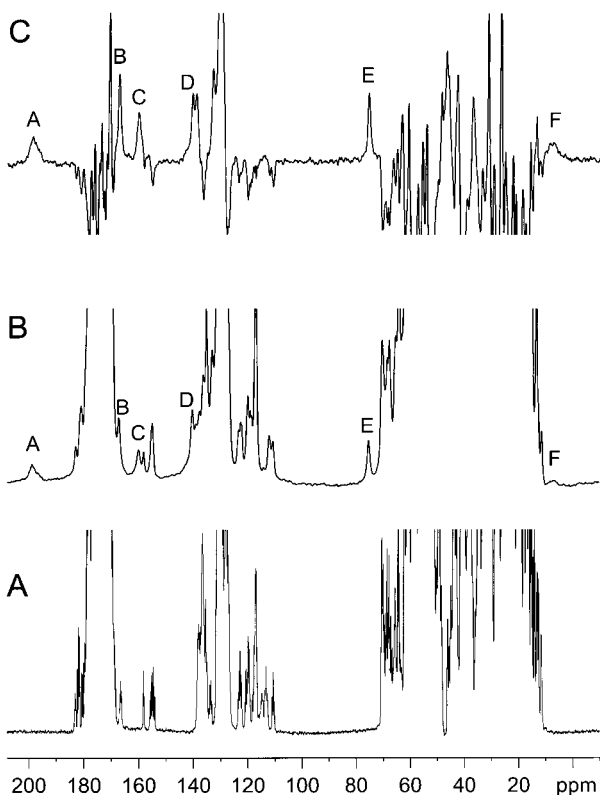


Figure 5. The 1-D ^{13}C -NMR spectra of *P. aeruginosa* azurin in 25 mM potassium phosphate buffer 95 : 5 $\text{H}_2\text{O} : \text{D}_2\text{O}$ at 40°C and pH 5.5. (A) A one-pulse experiment with proton decoupling, a repetition rate of 2 scans/s, 5-Hz line broadening, and the Cu(I) form of the protein; (B) a one-pulse experiment with proton decoupling, a repetition rate of 10 scans/s, 80-Hz line broadening, and the Cu(II) form of the protein; (C) inversion recovery experiment with proton decoupling, interscan delay of $\tau_0 = 100$ ms, a repetition rate of 3 scans/s, 80-Hz line broadening, and the Cu(II) form of the protein.

that additional paramagnetically shifted peaks are present that so far may have escaped detection due to the large line width. Signals A–F are broadened with respect to the majority of the signals detected, T_1 values determined by inversion-recovery experiments are in the range of 1–100 ms [Fig. 5(C)], and the resonance positions of five signals show a significant temperature dependence. The chemical shifts, T_1 values, slopes, and intercepts of Curie plots [$\delta^{\text{tot}} = f(1/T)$] for signals A–F are listed in Table III. Because the intercepts of a Curie plot ideally reflect the diamagnetic contribution to the observed shift, we propose that peaks A–C belong to ^{13}C in the carbonyl moieties, D originates from an aromatic side chain, and E and F are either from the backbone or an aliphatic side chain.

Thus far we have not been able to detect scalar sequence-specific correlations for any of the signals except D (Fig. 4); therefore, we cannot make definitive assignments. However, the following observations point toward the most probable candidates.

Peaks A and C

Because the complete \mathbf{g} tensor with respect to the molecular framework has been established by single crystal EPR,⁷¹ the expected dipolar shifts for each nucleus in the molecule can be calculated using Eq. (3) and the X-ray structure of Cu(II) azurin at pH 5.5 (Protein Data Bank code 4azu).⁸ Except for the directly coordinated atoms, the predicted dipolar shifts for the nuclei in the Cu ligands are less than ± 5 ppm and less than ± 2.5 ppm for noncoordinated residues. Despite the fact that the point–dipole approximation breaks down for nuclei close to the copper or sulfur atom of Cys 112 (which is expected to carry almost 30% of the electron spin density⁷²), the calculated values give a reasonable estimate for the maximum value of the dipolar contribution to the chemical shift. Therefore, the approximate 20 and -10 ppm shifts outside of the diamagnetic envelope observed for carbons A and C, respectively, are indicative of unpaired spin density at these nuclei. This fact limits the most plausible candidates for the assignment to CO groups of the five ligating residues and Asn 47, which is hydrogen bonded to the S^γ of Cys 112 through its peptide NH.⁸ Because we find both positive and negative paramagnetic shifts, the spin densities must also be positive or negative, thus pointing toward the presence of two different spin delocalization mechanisms^{46,48,49,54,73,74}: the spin density transfer characterized by attenuation of its intensity

Table III Experimental Chemical Shifts (δ^{tot}) and Longitudinal Relaxation Times (T_1) at 40°C

Peak	δ (ppm)	T_1 (ms)	Slope (K ppm $\times 10^{-3}$)	Intercept (ppm)
A	198.3	8	11.2	163.3
B	167.4	20	-3.0	176.9
C	160.3	<8	-6.0	179.2
D	140.5	85	0.1	140.3
E	75.4	66	3.0	65.9
F	9.1	<8	-16.7	61.4

The slopes and intercepts are of Curie plots [$\delta^{\text{tot}} = f(1/T)$] of the paramagnetic resonances observed in the 1-D ^{13}C -NMR spectra of the *P. aeruginosa* azurin.

with the increasing number of bonds and the spin polarization mechanism in which the sign of the spin density alternates between consecutive nuclei. Both mechanisms were proposed for the interpretation of the ^1H hyperfine shifts in the Co(II) and Ni(II) substituted *P. aeruginosa* azurin⁷⁵ and in oxidized Cu(II) spinach plastocyanin.⁴⁰

Peak B

A scalar correlation to C^α at 51.8 ppm can be seen in the [^{13}C - ^{13}C] 2-D correlation spectroscopy (COSY) experiment (data not shown); however, the resulting cross peak is quite weak and broad, and in triple resonance experiments no connectivity was observed. Because signal B is only slightly shifted outside of the diamagnetic envelope, the origin of the hyperfine shift cannot be unambiguously determined; but a very short T_1 indicates close proximity of the Cu(II).

Peak D

Peak D, which is located at 140.7 ppm, is minimally shifted outside of the aromatic carbon region, but in this case the combination of triple resonance experiments and the [^{13}C - ^{13}C] COSY experiment allows us to clarify its assignment. In a [^{13}C - ^{13}C] COSY spectrum signal D exhibits a connectivity to a resonance at 41.8 ppm [Fig. 6(A)]. Cross peaks in this region are characteristic for connectivities of the C^γ of an aromatic ring to C^β . The HNCACB experiment on the oxidized sample of *P. aeruginosa* azurin allowed us to define 7 out of 13 expected frequencies of C^β 's from the aromatic residues (Phe 15, 29, 97, and 110; Tyr 72 and 108; and His 83). A series of 2-D strips from the 3-D HNCACB spectrum used for the sequence-specific assignments of residues 106–110 is presented in Figure 7(A). Figure 7(B) contains the strips where frequencies corresponding to C^β 's can be unambiguously defined by either intra- (His 83, Phe 97) or interresidual (Asn 16 for Phe 15, Thr 30 for Phe 29, and Leu 73 for Tyr 72) connectivities. In this way peak D can be identified as a C^γ of Phe 15. The line width and a 2 ppm dipolar shift calculated from the comparison of the reduced with the oxidized form are both in agreement with the distance to the copper (7.4 Å) and an orientation similar to that observed in the X-ray structure.⁸ The remaining three cross peaks observed in Figure 6(A) are assigned to the Trp 48, His 35, and Phe 111 residues, based on their characteristic chemical shift for either C^γ (Trp 48) or C^β (His 35 and Phe 111). These assignments were additionally confirmed by com-

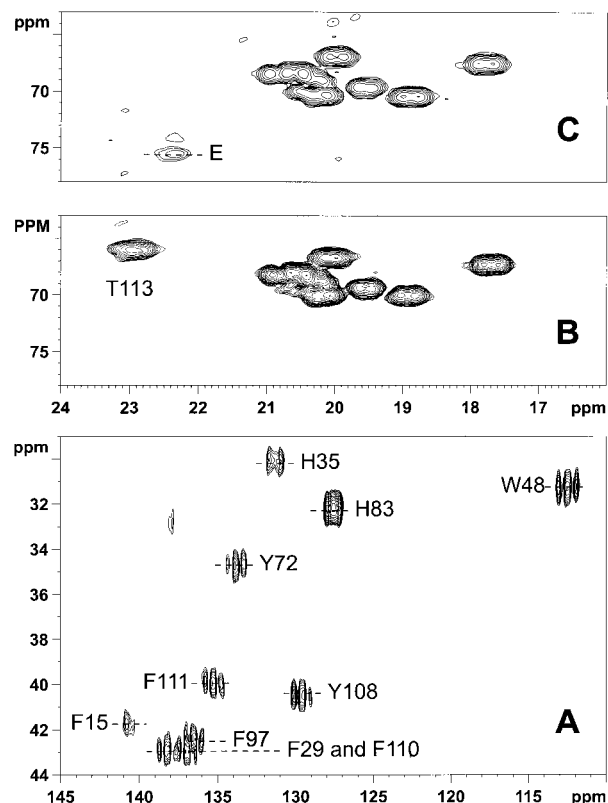


Figure 6. Regions of 2-D [^{13}C - ^{13}C] COSY spectra showing (A) C_β to C_γ connectivities of the aromatic rings in the oxidized azurin from *P. aeruginosa*, (B) C_β - C_γ connections for threonine residues in reduced azurin, and (C) oxidized azurin. Spectra were recorded for azurin samples in 25 mM potassium phosphate buffer 95 : 5 H_2O : D_2O at 40°C and pH 5.5.

parison with the data available for the diamagnetic form of *P. aeruginosa* azurin (data not shown).

Peak E

The identification of peak E can be achieved in a similar manner using a combination of triple resonance and [^{13}C - ^{13}C] COSY experiments. The combination of HNCACB and CBCA(CO)NH experiments for the reduced and oxidized forms of *P. aeruginosa* azurin allowed us to sequence specifically assign the C^β frequencies for all threonine residues with the exception of Thr 113 in the oxidized form. Threonine C^β and C^γ resonances are typically found in the ranges of 58–78 and 17–25 ppm, respectively,⁷⁶ and the C^β - C^γ cross peaks from threonine residues fall in a region where no other signals are expected. We utilized triple resonance experiments to assign the C^β of Thr 113 in the diamagnetic form of *P. aeruginosa*

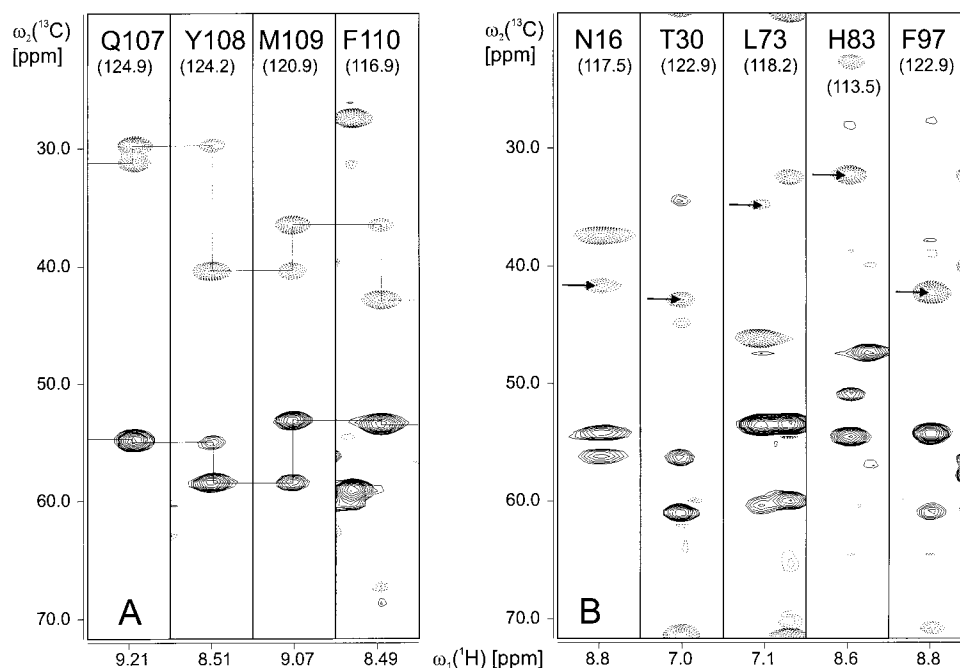


Figure 7. (A) A strip plot of HNCACB data that show the sequential connection for the resonances from (—) $^{13}\text{C}_\alpha$ and (---) $^{13}\text{C}_\beta$ nuclei of residues 106–110 of oxidized azurin from *P. aeruginosa*. (B) HNCACB strips for residues Asn 16, Thr 30, Leu 73, His 83, and Phe 97 that allow us to unambiguously define the C_β frequencies for aromatic residues by either intra- (His 83, Phe 97) or interresidual (Asn 16 for Phe 15, Thr 30 for Phe 29, and Leu 73 for Tyr 72) connectivities as indicated by arrows. The numbers in parentheses below the residue label correspond to the chemical shifts of the ^{15}N (ω_3), at which the ^1H - ^{13}C plane was defined. The 3-D spectrum was recorded for the azurin sample in 25 mM potassium phosphate buffer 95 : 5 H_2O : D_2O at 40°C and pH 5.5.

azurin at 67.9 ppm. Using the resonance assignment for the remaining nine threonines and a process of elimination, the assignment of the C_β - C_γ cross peak of Thr 113 in the [^{13}C - ^{13}C] COSY spectrum of the diamagnetic form was straightforward [Fig. 6(B)]. All threonine residues except Thr 113 are located far from the Cu(II) ion, hence in the *paramagnetic* state we expect no significant changes in their chemical shift or relaxation as observed by comparing Figure 6(B, C). In addition, a weak cross peak can be seen in Figure 6(C) between signal E in the ω_2 dimension and a position very close to the diamagnetic value of the $^{13}\text{C}_\gamma$ -Thr 113 in the ω_1 dimension. It is therefore tempting to assign this cross peak to the Thr 113 spin system of which the C_β resonance could not be detected in the triple resonance experiments. However, the almost 10 ppm difference in chemical shift with regard to the diamagnetic position cannot be justified simply on the basis of dipolar interaction with the unpaired electron. Results of recent W-band ENDOR⁷⁷ and NMR studies⁷⁵ on Co(II) and Ni(II) substituted *P. aeruginosa* azurin

indicate that the unpaired electron is significantly delocalized via a hydrogen bonding network to the backbone protons of Asn 47. The C_β of Thr 113 is separated from the copper ion by 7 covalent bonds and on a different “route” by 10 bonds including two hydrogen bridges involving Asn 47. Electrochemical studies⁷⁸ demonstrated a strong electrostatic interaction of the Asn 47 side chain with the metal center. Hence, the Thr 113 resonances may experience both paramagnetic and electrostatic effects, which will change upon oxidation or reduction of the copper.

Peak F

This signal is the most upfield shifted, paramagnetically affected peak thus far detected in the 1-D ^{13}C -NMR spectrum. The estimated T_1 value is the shortest (<8 ms) and its chemical shift demonstrates the greatest temperature dependence (-16.7×10^{-3} K ppm value of the slope from the Curie plot), indicating a significant amount of unpaired electron density. The upfield

shift, which is diagnostic for the presence of negative spin density, is similar to the one observed for the H^β of His 54 in the oxidized form of amicyanin from *Thiobacillus versutus*³⁸ or the H^β of His 37 and the H^α of Cys 84 in oxidized spinach plastocyanin.⁴⁰ Together with the intercept from the Curie plot of peak F, these facts support the tentative assignment of this signal to the C^α or C^β of one of the ligated residues.

CONCLUSIONS

We illustrated the application of 1H - and ^{13}C -NMR spectroscopy to copper proteins in their paramagnetic state by the study of two different, but closely related, electron transfer proteins. The electronic structure of the Cu_A center was analyzed by 1H -NMR. The spectrum of the Cu_A -CyoA was used as a basis for a comparison of the Cu_A site in different wild-type and engineered proteins. The analysis of the spin density distribution over the Cu_A ligands, in particular when considering the amount of spin density present on the histidine ligands, led to the conclusion that in the native Cu_A domains investigated so far, the two Cu ions tend to be magnetically equivalent, while in the engineered Cu_A constructs a tendency can be observed toward spin localization on one of the copper centers. The mechanistic properties of the native domains thus might reflect an evolutionary adaptation to facilitated electron transfer, which is not simple to mimic in engineered domains. Facilitated electron transfer was quoted as a possible mechanistic advantage of a Cu_A center over a type-1 blue copper center.^{31,32,50} Further, the shifts of the Cys H^β and their temperature dependence were analyzed. A reevaluation of the data on the Cu_A -*Pver* taking into account a much larger shift for the Cys220 H^β , which is in agreement with data reported by Luchinat et al.⁴⁵ on a similar domain from *P. denitrificans* and with data obtained from pulsed-ENDOR measurements, does not affect the conclusions of the previously reported analysis with respect to the thermal accessibility of the excited $^2B_{3u}$ electronic state. Additionally, significantly different spin densities on the cysteine ligands can be postulated from the outcome of the analysis.

The ^{13}C -NMR measurements were carried out on isotopically enriched azurin. The data reported showed that it is possible to observe hyperfine shifted signals in these spectra and to assign some of them. While this is a first attempt to

observe such signals in the ^{13}C -NMR spectrum of a blue copper protein by multidimensional techniques, further elaboration is needed. One of the remarkable findings is that the side chain of Thr 113, which is not involved in coordination of the metal, is clearly affected by the paramagnetism of the Cu(II) center, possibly through a hydrogen bonding network. Thus, ^{13}C -NMR of a paramagnetic small blue copper protein can contribute to mapping the finer details of the spin distribution over the first and second coordination sphere of the Cu.

Isolation of Proteins

The expression and purification of soluble domains of subunit II from cytochrome *c* oxidase from *P. versutus* and quinol oxidase from *E. coli* were carried out as described.^{19,20,24} The expression and purification of the isotopically enriched oxidized azurin from *P. aeruginosa* will be described elsewhere.

Sample Preparation

The Cu_A site containing a soluble domain from *P. versutus* and Cu_A -CyoA samples for NMR spectroscopy were concentrated to 3–5 mM and exchanged for 10 mM sodium phosphate buffer at pH 5.4 and 5.6, respectively, in either 99.98 or 10% D_2O . The 2 mM ^{13}C , ^{15}N -labeled sample of *P. aeruginosa* azurin was exchanged for 25 mM potassium phosphate buffer (pH 5.5) in 5% D_2O .

NMR Spectroscopy

All 1H - and ^{13}C -NMR spectra were recorded on a Bruker DMX 600-MHz spectrometer equipped with broadband and 1H , ^{13}C , and ^{15}N triple-resonance probe heads. The 1-D 1H -NMR spectra were measured by a one-pulse sequence with ^{13}C , ^{15}N decoupling if necessary. Elimination of the water signal was achieved either by presaturation or using the super-WEFT pulse sequence.³⁷ Steady-state 1-D 1H NOE measurements were performed as reported previously.²⁴ The 1-D ^{13}C -NMR spectra were recorded by using a one-pulse sequence with power gated decoupling. Fast repetition rates (up to 15 scans/s) were used to saturate the diamagnetic resonances. The spin lattice relaxation times, T_1 , of the hyperfine shifted ^{13}C resonances were determined by inversion recovery experiments. The interpulse delay τ_0 was varied between 1 and 200 ms. The T_1 values were

estimated from the null in the transient intensity $T_1 = \tau_0/\ln 2$ ($\pm 30\%$ error).

The direct detected 2-D [^{13}C - ^{13}C] COSY spectrum⁷⁹ was recorded over a 50-kHz spectral width and with a repetition rate of 4 scans/s. Broadband WALTZ-16 proton decoupling was applied.

The experimental conditions for the 3-D triple resonance experiments will be described elsewhere.

REFERENCES

- Adman, E. T. *Adv Protein Chem* 1991, 42, 145–197.
- Adman, E. T. In *Topics in Molecular and Structural Biology. Metalloproteins, Part 1*; Harrison, P. M., Ed.; Macmillan: London, 1985; p 1–42.
- Solomon, E. I.; Baldwin, M. J.; Lowery, M. D. *Chem Rev* 1992, 92, 521–542.
- Guss, J. M.; Freeman, H. C. *J Mol Biol* 1983, 169, 521–563.
- Baker, E. N. *J Mol Biol* 1988, 203, 1071–1095.
- Guss, J. M.; Merritt, E. A.; Phizackerley, R. P.; Hedman, B.; Murata, M.; Hodgson, K. O.; Freeman, H. C. *Science* 1988, 241, 806–811.
- Adman, E. T.; Turley, S.; Bramson, R.; Petratos, K.; Banner, D.; Tsernoglou, D.; Beppu, T.; Watanabe, H. *J Biol Chem* 1989, 264, 87–99.
- Nar, H.; Messerschmidt, A.; Huber, R.; Van de Kamp, M.; Canters, G. W. *J Mol Biol* 1991, 221, 765–772.
- Romero, A.; Nar, H.; Huber, R.; Messerschmidt, A.; Kalverda, A.; Canters, G. W.; Durley, R.; Mathews, F. S. *J Mol Biol* 1994, 236, 1196–1211.
- Moore, J. M.; Case, D. A.; Chazin, W. J.; Gippert, G. P.; Havel, T. F.; Powls, R.; Wright, P. E. *Science* 1988, 240, 314–317.
- Moore, J. M.; Lepre, C. A.; Gippert, G. P.; Chazin, W. J.; Case, D. A.; Wright, P. E. *J Mol Biol* 1991, 221, 533–555.
- Bagby, S.; Driscoll, P. C.; Harvey, T. S.; Hill, H. A. O. *Biochemistry* 1994, 33, 6611–6622.
- Kalverda, A. P.; Wymenga, S. S.; van de Ven, F. J. M.; Hilbers, C. W.; Canters, G. W. *J Mol Biol* 1994, 240, 358–371.
- Roberts, V. A.; Fisher, C. L.; Redford, S. M.; McRee, D. E.; Parge, H. E.; Getzoff, E. D.; Tainer, J. A. *Free Rad Res Commun* 1991, 12–13, 269–278.
- Rompel, A.; Fischer, H.; Meiwes, D.; Büldt-Karentzopoulos, K.; Dillinger, R.; Tuzek, F.; Witzel, H.; Krebs, B. *J Biol Inorg Chem* 1999, 4, 5663.
- Messerschmidt, A.; Rossi, A.; Ladenstein, R.; Huber, R.; Bolognesi, M.; Gatti, G.; Marchesini, A.; Petruzzelli, R.; Finazzi-Agro, A. *J Mol Biol* 1989, 206, 513–529.
- Stevens, T. H.; Martin, C. T.; Want, H.; Brudvig, G. W.; Scholes, C. P.; Chan, S. J. *J Biol Chem* 1982, 257, 12106–12113.
- Kroneck, P. M. H.; Antholine, W. E.; Kastrau, D. H. W.; Buse, G.; Steffens, G. C.; Zumft, W. G. *FEBS Lett* 1990, 268, 274–276.
- van der Oost, J.; Lappalainen, P.; Musacchio, A.; Warne, A.; Lemieux, R.; Rumbley, J.; Gennis, R. B.; Aasa, R.; Pascher, T.; Malmstrom, B. G.; Saraste, M. *EMBO J* 1992, 11, 3209–3217.
- Kelly, M.; Lappalainen, P.; Talbo, G.; Haltia, T.; van der Oost, J.; Saraste, M. *J Biol Chem* 1993, 268, 16781–16787.
- van Wachenfeldt, C.; de Vries, S.; van der Oost, J. *FEBS Lett* 1994, 340, 109–113.
- Slutter, C. E.; Sanders, D.; Wittung, P.; Malmström, B. G.; Aasa, R.; Richards, J. H.; Gray, H.; Fee, J. A. *Biochemistry* 1996, 35, 3387–3395.
- Lappalainen, P.; Aasa, R.; Malmström, B. G.; Saraste, M. *J Biol Chem* 1993, 268, 26416–26421.
- Salgado, J.; Warmerdam, G.; Bubacco, L.; Canters, G. W. *Biochemistry* 1998, 37, 7378–7389.
- Saraste, M. *Q Rev Biophys* 1990, 23, 331–366.
- Dennison, C.; Vijgenboom, E.; de Vries, S.; van der Oost, J.; Canters, G. W. *FEBS Lett* 1995, 365, 92–94.
- Hay, M.; Richards, J. H.; Lu, Y. *Proc Natl Acad Sci USA* 1996, 93, 461–464.
- Solomon, E. I.; Lowery, M. D. *Science* 1993, 259, 1579–1581.
- Guckert, J. A.; Lowery, M. D.; Solomon, E. I. *J Am Chem Soc* 1995, 117, 2817–2844.
- Farrar, J. A.; Neese, F.; Lappalainen, P.; Kroneck, P. M. H.; Saraste, M.; Zumft, W. G.; Thomson, A. J. *J Am Chem Soc* 1996, 118, 11501–11514.
- Gamelin, D. R.; Randal, D. W.; Hay, M. T.; Houser, T. C. M.; Canters, G. W.; de Vries, S.; Tolman, W. B.; Lu, Y.; Solomon, E. I. *J Am Chem Soc* 1998, 120, 5246–5263.
- Achim, C.; Bominaar, E. L.; Münck, E. *J Biol Inorg Chem* 1998, 3, 126–134.
- Robin, M. B.; Day, P. *Adv Inorg Chem Radiochem* 1967, 10, 247–422.
- Kroneck, P. M. H.; Antholine, W. E.; Riester, J.; Zumft, W. G. *FEBS Lett* 1988, 242, 70–74.
- Antholine, W. E.; Kastrau, D. H. W.; Steffens, G. C. M.; Buse, G.; Zumft, W. G.; Kroneck, P. M. H. *Eur J Biochem* 1992, 209, 875–881.
- Bertini, I.; Turano, P.; Vila, A. J. *Chem Rev* 1993, 93, 2833–2932.
- Inubushi, T.; Becker, E. D. *J Magn Reson* 1983, 51, 128–133.
- Kalverda, A. P.; Salgado, J.; Dennison, C.; Canters, G. W. *Biochemistry* 1996, 35, 3085–3092.
- Salgado, J.; Kalverda, A. P.; Canters, G. W. *J Biomol NMR* 1997, 9, 299–305.
- Bertini, I.; Ciurli, S.; Dikiy, A.; Gasanov, R.; Luchinat, C.; Martini, G.; Safarov, N. *J Am Chem Soc* 1999, 121, 2037–2046.
- Pfenninger, S.; Antholine, W. E.; Barr, M. E.; Hyde, J. S.; Kroneck, P. M. H.; Zumft, W. G. *Biophys J* 1995, 69, 2761–2769.
- Bertini, I.; Bren, K. L.; Clemente, A.; Fee, J. A.;

- Gray, H. B.; Luchinat, C.; Malmström, B. G.; Richards, J. H.; Sanders, D.; Slutter, C. E. *J Am Chem Soc* 1996, 118, 11658–11659.
43. Dennison, C.; Berg, A.; de Vries, S.; Canters, G. W. *FEBS Lett* 1996, 394, 340–344.
44. Dennison, C.; Berg, A.; Canters, G. W. *Biochemistry* 1997, 36, 3262–3269.
45. Luchinat, C.; Soriano, A.; Djinovic-Carugo, K.; Saraste, M.; Malmström, B. G.; Bertini, I. *J Am Chem Soc* 1997, 119, 11023–11027.
46. Bertini, I.; Luchinat, C. In *Coordination Chemistry Reviews*; Lever, A. B., Ed.; Elsevier: Amsterdam, 1996; Vol. 150, p 1–300.
47. Kurland, R. J.; McGarvey, B. R. *J Magn Reson* 1970, 2, 286–301.
48. La Mar, G. N. In *NMR of Paramagnetic Molecules; Principles and Applications*; LaMar, G. N.; Horrocks, W. D., Jr.; Holm, R. H., Eds.; Academic Press: New York, 1973; p 85–126.
49. Bertini, I.; Luchinat, C. *NMR of Paramagnetic Molecules in Biological Systems*; Benjamin Cummings; Menlo Park, CA, 1986.
50. Larsson, S.; Kaellebring, B.; Wittung, P.; Malmström, B. G. *Proc Natl Acad Sci USA* 1995, 92, 7167–7171.
51. Neese, F.; Zumft, W. G.; Antholine, W. E.; Kroneck, P. M. H. *J Am Chem Soc* 1996, 118, 8692–8699.
52. Neese, F.; Kappl, R.; Hüttermann, J.; Zumft, W. G.; Kroneck, P. M. H. *J Biol Inorg Chem* 1998, 3, 53–67.
53. Andrew, C. R.; Lappalainen, P.; Saraste, M.; Hay, M. T.; Lu, Y.; Dennison, C.; Canters, G. W.; Fee, J. A.; Slutter, C. E.; Nakamura, N.; Sanders-Loehr, J. *J Am Chem Soc* 1995, 117, 10759–10760.
54. de Boer, E.; Colpa, J. P.; Lazdins, D.; Karplus, M. *J Chem Phys* 1967, 47, 3098–3100.
55. Gurbiel, R. J.; Fann, Y. C.; Surerus, K. K.; Werst, M. M.; Musser, S. M.; Doan, P. E.; Chan, S. I.; Fee, J. A.; Hoffman, B. M. *J Am Chem Soc* 1993, 115, 10888–10894.
56. Wilmanns, M.; Lappalainen, P.; Kelly, M.; Sauer-Eriksson, E.; Saraste, M. *Proc Natl Acad Sci USA* 1995, 92, 11955–11959.
57. Farrar, J. A.; Lappalainen, P.; Zumft, W. G.; Saraste, M.; Thomson, A. J. *Eur J Biochem* 1995, 232, 294–303.
58. Iwata, S.; Ostermeier, C.; Ludwig, B.; Michel, H. *Nature* 1995, 376, 660–669.
59. Wittekind, M.; Mueller, L. *J Magn Reson B* 1993, 101, 201–205.
60. Kay, L. E.; Ikura, M.; Tschudin, R.; Bax, A. *J Magn Reson* 1990, 89, 496–514.
61. Farmer, B. T.; Venters, R. A.; Spicer, L. D.; Wittekind, M. G.; Müller, L. *J Biomol NMR* 1992, 2, 195–202.
62. Grzesiek, S.; Bax, A. *J Am Chem Soc* 1992, 114, 6291–6293.
63. Muhandiram, D. R.; Kay, L. E. *J Magn Reson B* 1994, 103, 203–216.
64. Kalverda, A. P. Ph.D. Thesis, University of Leiden, The Netherlands, 1996.
65. Adman, E. T.; Canters, G. W.; Hill, H. A. O.; Kitchen, N. A. *FEBS Lett* 1982, 143, 287–292.
66. Ugurbil, K.; Mitra, S. *Proc Natl Acad Sci USA* 1985, 82, 2039–2043.
67. van de Kamp, M.; Hali, F. C.; Rosato, N.; Finazzi Agro, A.; Canters, G. W. *Biochim Biophys Acta* 1990, 1019, 283–292.
68. van de Kamp, M.; Canters, G. W.; Andrew, C. R.; Sanders-Loehr, J.; Bender, C. J.; Peisach, J. *Eur J Biochem* 1993, 218, 229–238.
69. Corin, A. F.; Bersohn, R.; Cole, P. E. *Biochemistry* 1983, 22, 2032–2038.
70. Salgado, J.; Jimenez, H. R.; Donaire, A.; Moratal, J. M. *Eur J Biochem* 1995, 231, 358–369.
71. Coremans, J. W. A.; Poluektov, O. G.; Groenen, E. J. J.; Canters, G. W.; Nar, H.; Messerschmidt, A. *J Am Chem Soc* 1994, 116, 3097–3101.
72. Larsson, S.; Broo, A.; Sjölin, L. *J Phys Chem* 1995, 99, 4860–4865.
73. Bertini, I.; Capozzi, F.; Luchinat, C.; Piccioli, M.; Vila, A. J. *J Am Chem Soc* 1994, 116, 651–660.
74. Bertini, I.; Donaire, A.; Felli, I. C.; Luchinat, C.; Rosato, A. *Inorg Chem* 1997, 36, 4798–4803.
75. Donaire, A.; Salgado, J.; Moratal, J. M. *Biochemistry* 1998, 37, 8659–8673.
76. The BioMagResBank data base can be found at <http://www.bmrb.wisc.edu/>.
77. Coremans, J. W. A.; Poluektov, O. G.; Groenen, E. J. J.; Canters, G. W.; Nar, H.; Messerschmidt, A. *J Am Chem Soc* 1996, 118, 12141–12153.
78. Hoitink, C. Ph.D. Thesis, University of Leiden, The Netherlands, 1993.
79. Nagayama, K.; Kumar, A.; Wüthrich, K.; Ernst, R. R. *J Magn Reson* 1980, 40, 321–329.